Supporting Information

Modulating intramolecular electron and proton transfer kinetics for promoting carbon dioxide conversion

Yajie Yuan,[a, b] Yazhen Zhao,[b] Shuai Yang,[c] Sheng Han,[*a] Chenbao Lu,[*b] Huiping Ji,[*b] Tianfu Wang,[b] Changchun Ke,[*d] Qing Xu,[e] Jinhui Zhu,[b,f] Xiaodong Zhuang[b]

[a] *School of Chemical and Environmental Engineering, Shanghai Institute of Technology, Shanghai 201418, China. E–mail: hansheng654321@sina.com (S. Han)*

[b] *The meso–Entropy Matter Lab, State Key Laboratory of Metal Matrix Composites, School of Chemistry and Chemical Engineering, Frontiers Science Center for Transformative Molecules, Shanghai Jiao Tong University, Shanghai 200240, China. E–mail: huiping.ji@sjtu.edu.cn; castle@sjtu.edu.cn (C. Lu)*

[c] *Shanghai Institute of Applied Physics, Chinese Academy of Sciences, Shanghai 201210, P. R. China*

[d] *Institute of Fuel Cells, School of Mechanical Engineering, Shanghai Jiao Tong University, Shanghai 200240, China. E–mail: kechangchun@sjtu.edu.cn (C. Ke)*

[e] *CAS Key Laboratory of Low-Carbon Conversion Science and Engineering, Shanghai Advanced Research Institute, Chinese Academy of Sciences, Shanghai 201210, P. R. China*

[f] *College of Chemistry, Zhengzhou University, Zhengzhou, Henan 450001, China*

1. Equipment and measurement

X-ray photoemission spectroscopy (XPS) measurements were performed on a PHI–5000C ESCA system, the C 1s value was set at 284.8 eV for charge corrections. The Raman spectra of samples were obtained on Lab-RAM HR800 with excitation by an argon ion laser (532 nm). XANES and EXAFS measurements were tested on the BL14W1 beamline at Shanghai Synchrotron Radiation Facility (SSRF). Fourier-transform infrared spectroscopy (FTIR) were recorded with a Spectrum 100 spectrometer (Perkin Elmer, Spectrum 100). Ultraviolet photoelectron spectroscopy (UPS) measurements were performed on ESCALAB 250xi with an unfiltered HeI (40 eV) gas discharge lamp under $2*10^{-8}$mbar. The cyclic voltammetry (CV) experiment was performed with recrystallized tetra-nbutyl-ammonium hexafluorophosphate ($TBAPF_6$, 0.1M) as supporting electrolyte at 298 K using the CH instrument (CHI 660E) electrochemical workstation.

2. Reagents

Tropolone, tosyl chloride, triethylamine, tert-butylamine, ethyl cyanoacetate, bis(pinacol) diboron, p-bromobenzaldehyde, potassium carbonate, iron chloride tetrahydrate, anhydrous magnesium sulfate, potassium acetate, acetic acid, bromine, [1,1'-bis (diphenylphosphino) ferrocene] dichloropalladium (II), tetrakis (triphenylphosphine) Palladium and nitrobenzene were purchased from Sinopharm Chemical Reagent. Toluene, ethanol, tetrahydrofuran, N,N-dimethylformamide, dichloromethane were purchased from Sigma-Aldrich. Pyrrole was purchased from Aladdin Reagent. All chemicals and solvents were used without further purification.

3. Synthesis details

3.1 Synthesis of compound 2

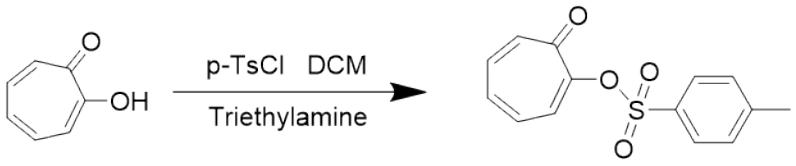

1 2

Under nitrogen atmosphere, tropolone 1 (5.00g, 40.94mmol, 1.0eqv) and tosyl chloride (7.81g, 40.94 mmol, 1.0 eqv) were added into a 250mL three-necked flask, added 60 mL CH_2Cl_2 to dissolve the solids, and then NEt dropwise (5.71 mL, 40.94 mmol, 1.0 eqv) was added. After stirring for 38 hours, the reaction was quenched with water to obtain a yellow slurry. Extracted with CH_2Cl_2 (3×100 mL), dried with anhydrous $MgSO_4$, filtered and concentrated under reduced pressure to obtain 7-oxocyclohepta-1,3,5-trien-1-yl4 - Methylbenzene sulfonate 2 (10.30 g, 90%, yellow crystalline solid).

3.2 Synthesis of compound 3

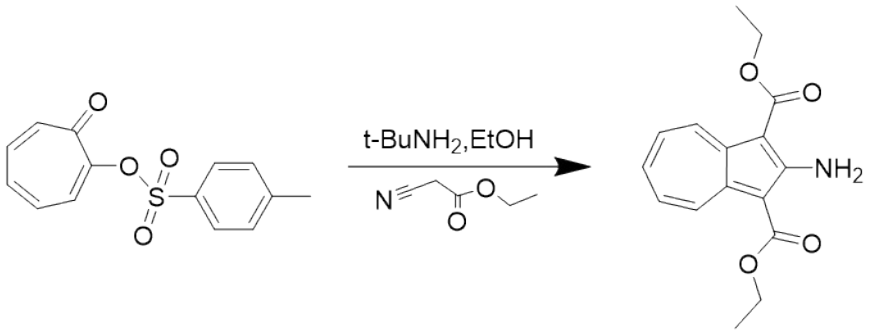

2 3

7-oxepan-1,3,5-trien-1-yl 4-methylbenzenesulfonate 2 (4.50 g, 16.29 mmol, 1.0 eqv) and ethyl cyanoacetate (3.82 mL, 35.83 mmol, 2.2 eqv) were added into a 500 mL flask and cooled to 0°C. Then, the tert-butylamine (4.28 mL, 40.72 mmol, 2.5 eqv) was dropwise into the above solution. After stirring the solution for 19 hours, an orange precipitated product was formed. A part of bright yellow products was obtained by filtration. The filtrates were concentrated under reduced pressure to about 30 mL, then, ice water (100 mL) was added to further precipitate the product, filtered and washed with water to obtain a part of dark yellow product, dried under vacuum. The crude product was purified by column chromatography and eluted with dichloromethane to obtain diethyl 2-aminoaza-1,3-dicarboxylate 3 (3.50g, 75%) as a bright orange solid.

3.3 Synthesis of compound 4

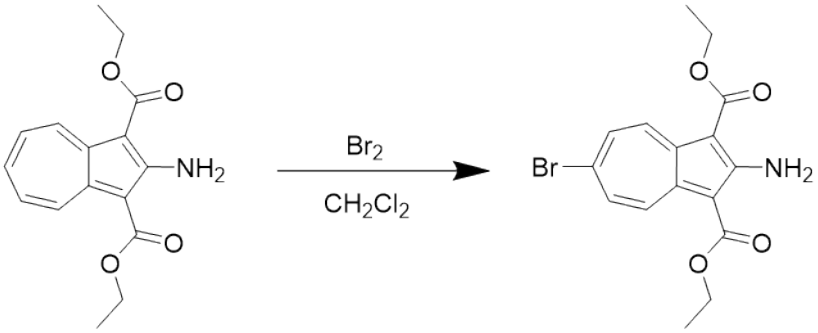

3 4

Diethyl 2-aminoazulene-1,3-dicarboxylate 3 (1.00 g, 3.48 mmol, 1.0 eqv) was dissolved in anhydrous CH2Cl2 (20 mL) and cooled to 0°C, and the bromine (0.20 mL, 3.83 mmol, 1.1 eqv) was slowly added dropwise. The solution was warmed to room temperature and stirred for 1 hour, then water (150 mL) was added and stirred for 1 to 2 hours to quench the reaction. The organic layer was separated by extraction, and then the aqueous layer was extracted with CH_2Cl_2 (2×50 mL). The collected organic extracts were dried with $MgSO_4$, filtered and concentrated under reduced pressure. The crude product was purified by column chromatography and eluted with dichloromethane to obtain diethyl 2-amino-6-bromoaza-1,3-dicarboxylate 4 as a brown crystalline solid (1.2 g, 95%).

3.4 Synthesis of compound 5

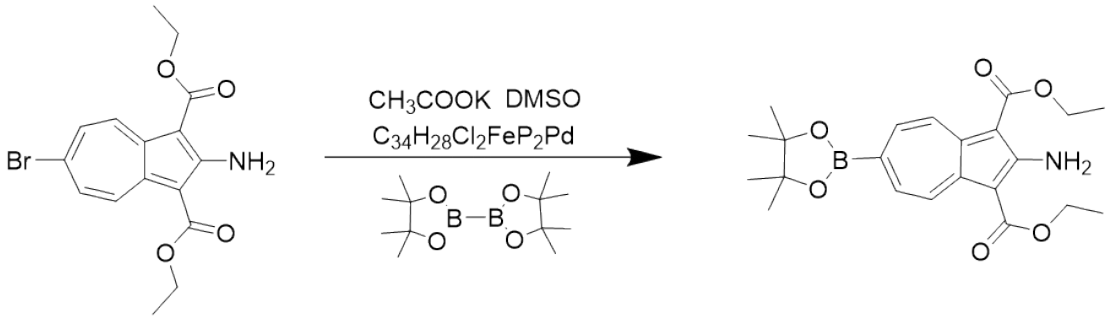

4 5

Under nitrogen atmosphere, 2-amino-6-bromoaza-1,3-dicarboxylic acid xylene 4 (6.50 g, 17.75 mmol, 1.00 eqv), [1,1'-bis (diphenylphosphino) ferrocene] dichloropalladium (II) (0.65 g, 0.89 mmol, 0.05 eqv), bis(pinacol) diboron (4.96 g, 19.53 mmol, 1.10 eqv) and potassium acetate (5.23 g, 52.25 mmol), 3.00 eqv) were added to a 250mL three-necked flask, and then anhydrous DMSO (60 mL) was added. The mixture was heated at 80°C for 18 hours. After cool to room temperature, the mixture was diluted with water (100 mL) then extracted with CH_2Cl_2 (4 × 50 mL). The combined organic extracts were washed with water (200 mL), dried over $MgSO_4$, filtered and concentrated under reduced pressure. Anion to obtain 2-amino-6-(4,4,5,5-tetramethyl-1,3,2-dioxaborolan-2-yl)azulene-1,3dicarboxylate (5.2 g, 71%) 5 was obtained as a bright orange solid.

3.5 Synthesis of Brpor

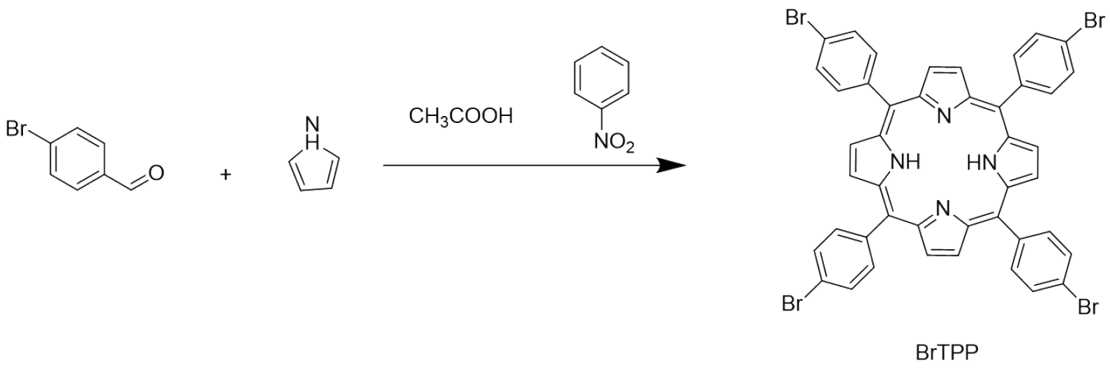

BrTPP

Dissolve p-bromobenzaldehyde (3.72g, 20mmol) in nitrobenzene (100mL) and acetic acid (150mL), heated the solution to 120 °C and added freshly distilled pyrrole (1.4mL, 20mmol) into the mixture. The reaction mixture was stirred at 120 °C for 1 h and then cooled to room temperature. The resulting dark purple precipitate was collected by filtration and washed with methanol (50 mL×3). The crude product was purified by column chromatography and eluted with dichloromethane to obtain 5,10,15,20-tetra (4'-bromophenyl) porphyrin (BrTPP) as a purple crystalline powder (1.92g) with a yield of 42%.

3.6 Synthesis of TAPP

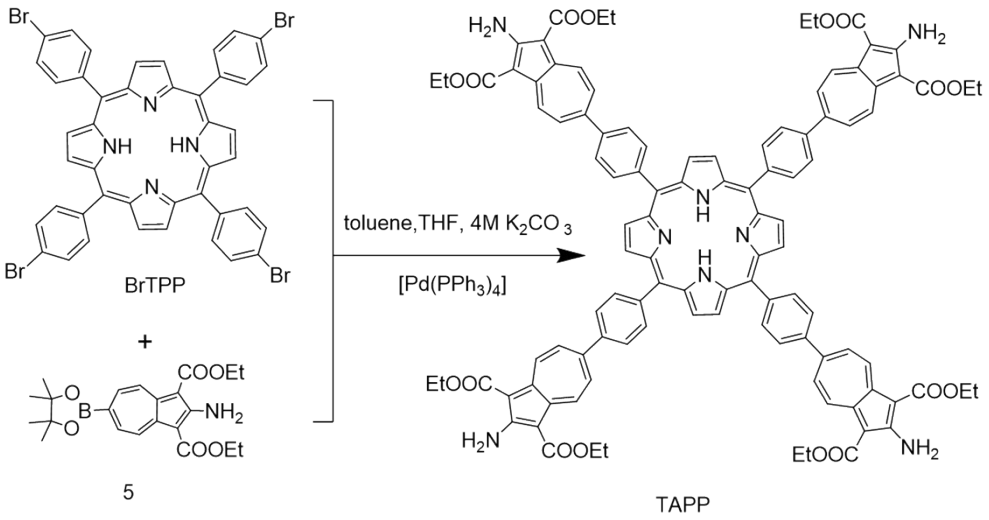

5,10,15,20-tetra(4'-bromophenyl) porphyrin (0.2 g, 0.21 mmol, 1.00 eqv), compound 5 (0.44 g, 1.07 mmol, 5.00 eqv) and tetrakis (triphenylphosphine) palladium $[Pd(PPh_3)_4]$ (12.42 mg, 0.01 mmol, 0.05 eqv) were added into a 50 mL double-necked round flask. Anhydrous toluene (16 mL), anhydrous THF (8 mL) and 4 M K_2CO_3 aqueous solution (4 mL) were added to the flask under N_2 atmosphere. The solution was heated at 80°C and stirred under N2 for 48 hours. After the mixture was cooled to room temperature, filtered with suction, and the filter residue was washed with dichloromethane to obtain 5,10,15,20-tetrakis (4'-(1,3-diesteryl, 6-amino) azulenylphenyl) porphyrin (TAPP) as a reddish brown powder without further purification. The yield was: 141mg, 37.4%.

3.7 Synthesis of FeTAPP

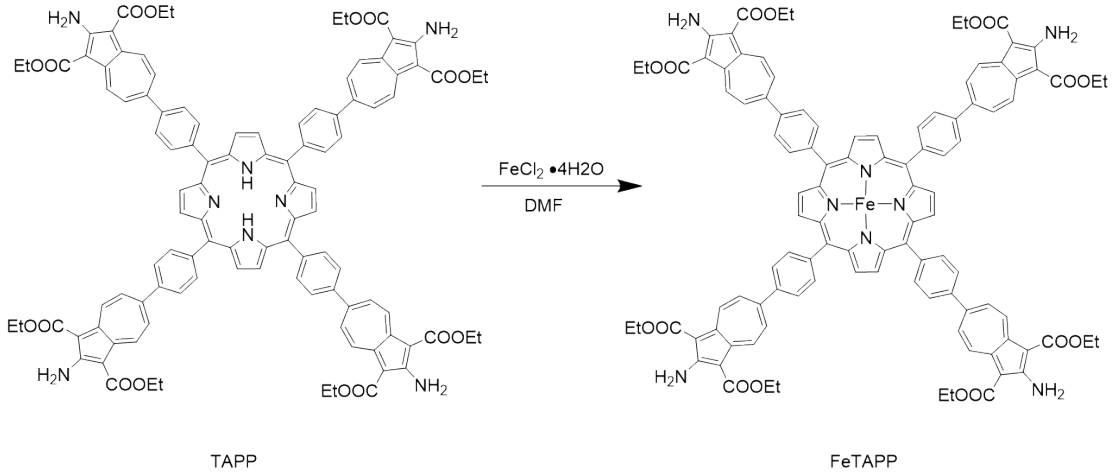

TAPP (50 mg, 28.47 mmol, 1.00 eqv) and excess iron (II) chloride tetrahydrate (33.97 mg, 170.85 mmol, 6.00 eqv) were added into a 500 mL double-necked round bottle. Then, added 200 mL of N,N-dimethylformamide to the flask under nitrogen atmosphere, heated and stirred at 140°C. After distillation under reduced pressure, the dissolved solids were added, extracted and washed, the organic layer was separated, dried with anhydrous $MgSO_4$, filtered, and concentrated under reduced pressure without further purification to obtain Fe centered TAPP (FeTAPP) powder. Yield: 41 mg, 79%.

3.8. CO_2 electroreduction measurement

3.8.1 Working electrode preparation

To improve the conductivity, the materials were mixed with carbon nanotubes (FB9110) to prepare the catalysis ink. Typically, 1 mg of FeTAPP and 9 mg of carbon nanotubes were dispersed in 1 mL of 0.5 wt.% Nafion solution and sonicated for 1 hour and then stirred overnight to form a uniform catalyst ink. Then drop 100 μL of catalyst ink on carbon paper (1 cm^{-2}) to achieve a catalyst loading of 1 mg^{-2}. It is prepared in the same ratio and procedure for FeTPP, CoTAPP and CoTPP.

3.8.2 Electrochemical measurements

The electrocatalytic CO_2 reduction performance test was carried out in a three-electrode H-type cell, in which Ag/AgCl was used as the reference electrode, Pt sheet was used as the counter electrode, and the catalyst loaded on carbon paper was used as the working electrode. The electrolyte was 0.5 M $KHCO_3$ saturated with CO_2. All potentials reported in this work were versus to the reversible hydrogen electrode (RHE) as following formula:

E_{RHE} (V) = E_{Ag} / AgCl (V) + 0.197 V + 0.0591V * pH

Before electrochemical polarization, CO_2 was continuously purged (20 mL min^{-1}) for 30 minutes and continued for the whole electrolysis process. The LSV curves were obtained at a scan rate of 5 mV s^{-1}, and all potentials in this study were without iR compensated.

The gaseous products were monitored by an online gas chromatograph (GC, Shimadzu GC2014C) equipped with a thermal conductivity detector (TCD) for H_2 and a flame ionization detector (FID) detector for CO quantification. The GC run Repeats every 18 minutes. Before product measurement, the GC is calibrated using standard gas mixtures (air liquid, CO, H_2, CH_4, C_2H_4, C_2H_6, C_2H_2 in N_2).

The liquid products in the $KHCO_3$ solution was analyzed and quantified through a Bruker 500 MHZ (AVANCE Ⅲ) NMR spectroscope with water suppression. After electrolysis, $KHCO_3$ electrolyte (0.5 mL) was collected and mixed with D_2O (0.1 mL) in an NMR tube and dimethyl sulfoxide (DMSO, 0.05 μL) as an internal standard.

3.8.3 Calculation

Faraday efficiency calculation (FE)

The Faraday efficiency of CO and H2 is calculated by the following formula:

$$FE = \frac{Q_i}{Q_{total}} = \frac{2 \times P_0 \times F \times \upsilon \times \upsilon^i}{R \times T \times I}$$ equation S1

where Q_i is the amount of charge required to generate the corresponding product i. Q_{total} is the amount of charge required to generate all products. 2 is the number of electrons transferred per mole of CO_2 to CO or per mole of H_2O transferred to H_2. P_0 is the atmospheric pressure (1.01×10^5 Pa), F is the Faraday constant (96485 C mol-1), v is the gas flow rate measured by a flow meter, and vi is the volume concentration of gas products in the waste gas of the electrolytic cell, determined by online GC. T is the reaction temperature (298.15 K), R is the target gas constant (8.314 J mol^{-1} K^{-1}), and I is the current at each potential.

Turnover frequency calculation (TOF)

The turnover frequency of product CO is calculated by the following formula:

$$TOF = \frac{FE_{CO} \times j_{total} \times A \times M_{Fe} \times t}{n \times F \times \omega_{Fe} \times m}$$ equation S2

where FE is the Faraday efficiency of CO, j_total is the total current density, A (1 cm^2) is the geometric area of the electrode, ω_{Fe} is the mass fraction of iron on the catalyst, m is the mass of the catalyst supported on the working electrode, and M_{Fe} is the cobalt The atomic mass of (56 g mol^{-1}). F is the Faraday constant (96485 C mol^{-1}), t is the reaction time (1 h / 3600 s), n is the number of electrons transferred to form the product, which is 2 for CO.

4. Analytical Data

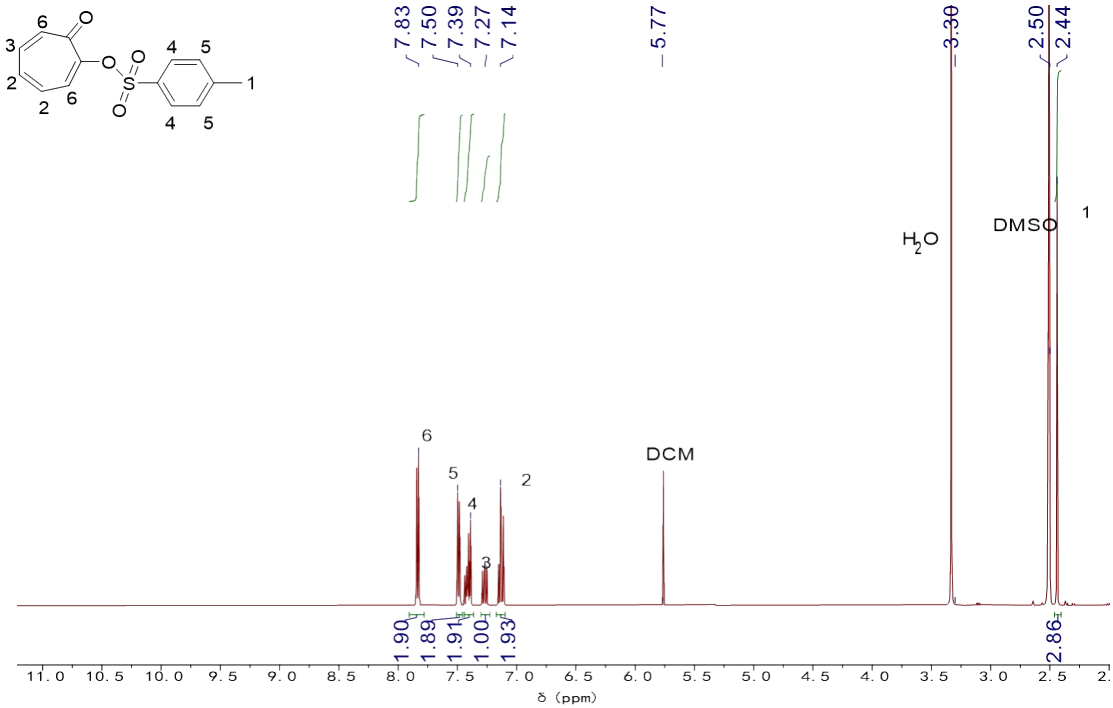

Fig. S1. ^{1}H NMR spectrum of compound 2 in DMSO-d_6 at 298K.

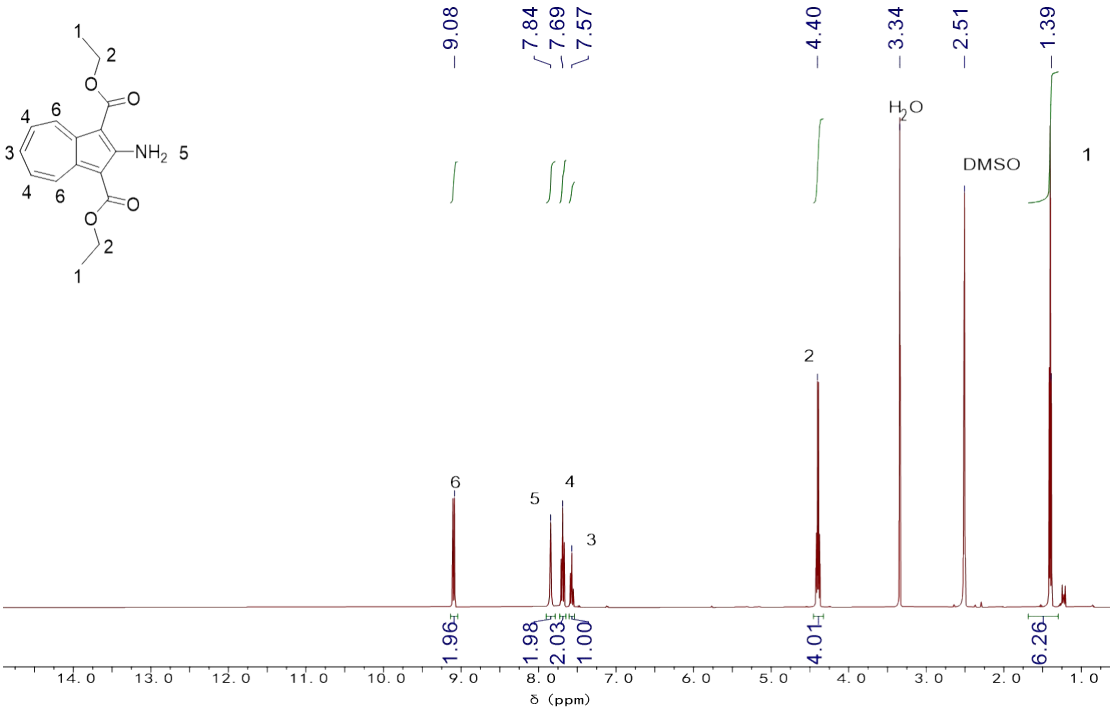

Fig. S2. ^{1}H NMR spectrum of compound 3 in DMSO-d_6 at 298K.

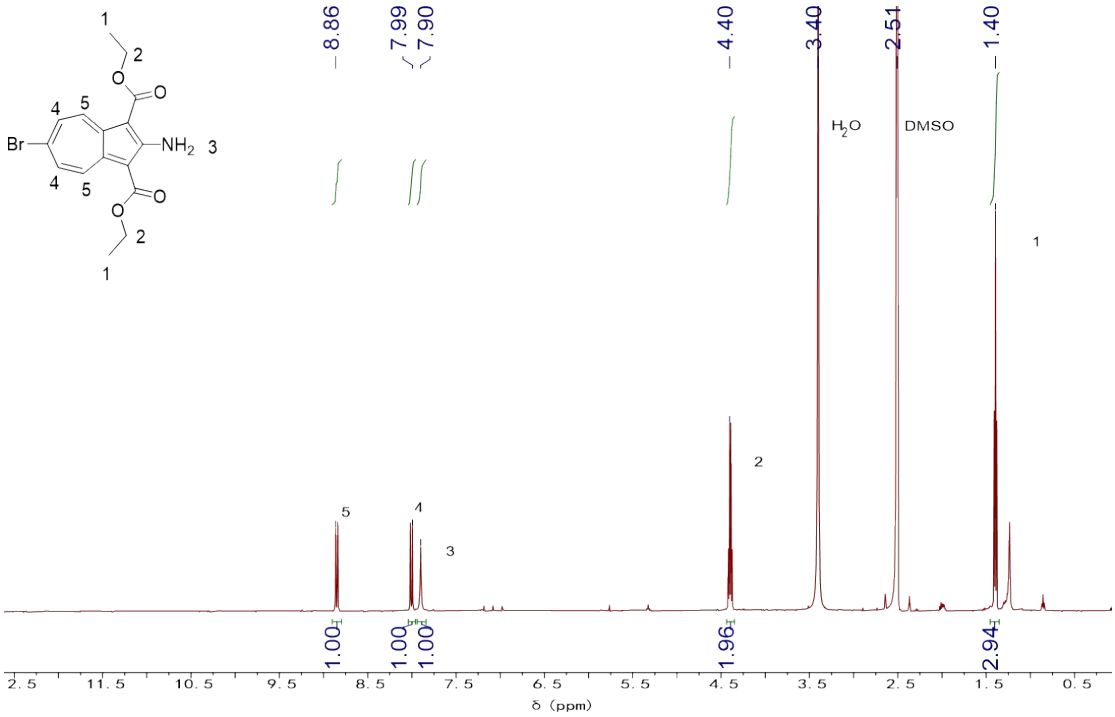

Fig. S3. ^{1}H NMR spectrum of compound 4 in DMSO-d_6 at 298K.

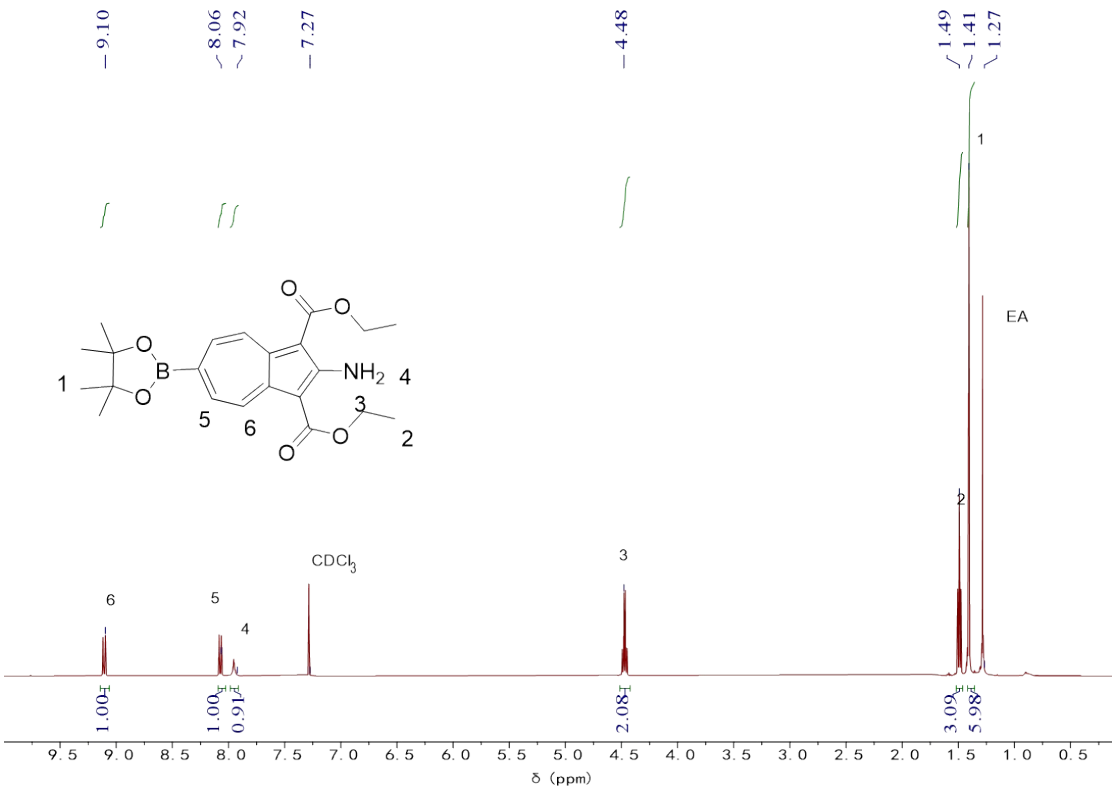

Fig. S4. ^{1}H NMR spectrum of compound 5 in $CDCl_3$ at 298K.

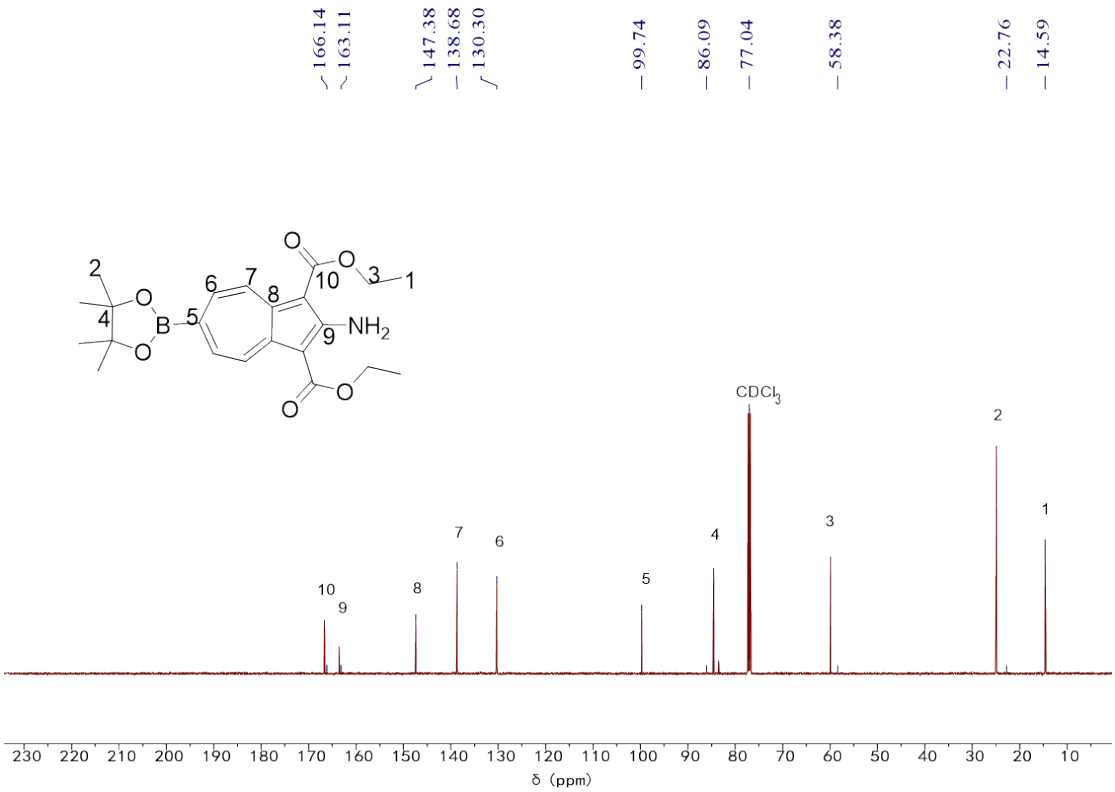

Fig. S5. ^{13}C NMR spectrum of compound 5 in $CDCl_3$ at 298K.

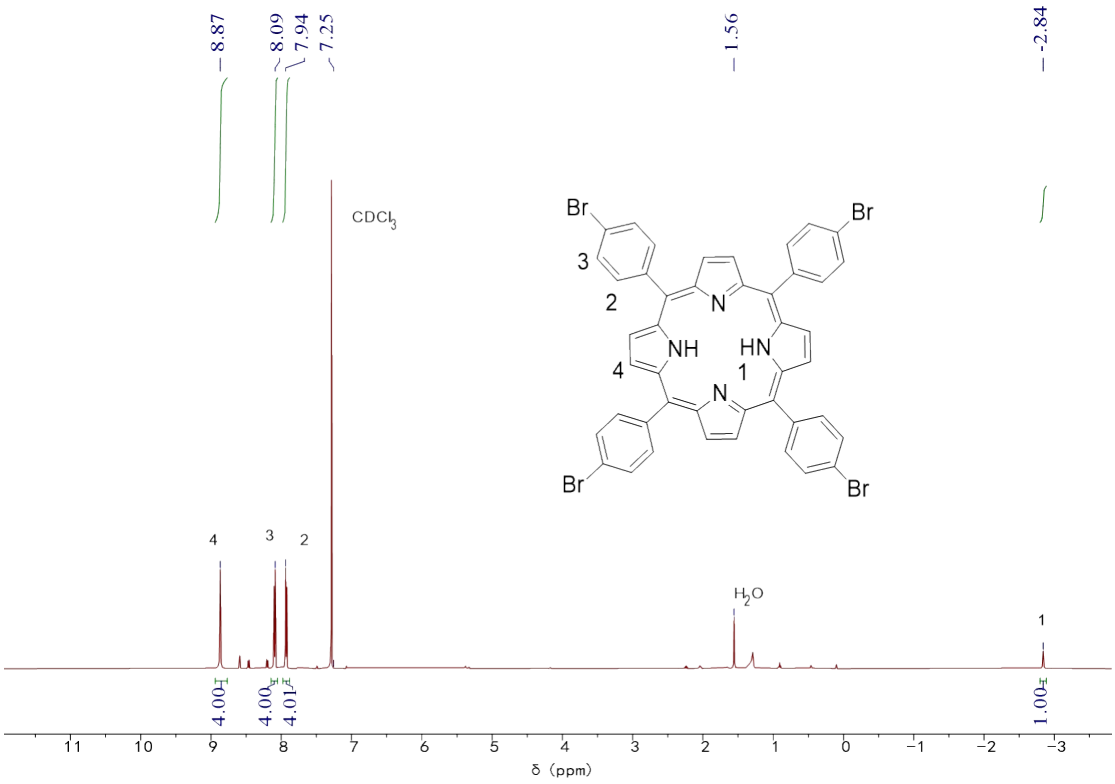

Fig. S6. ^{1}H NMR spectrum of BrTPP in $CDCl_3$ at 298K.

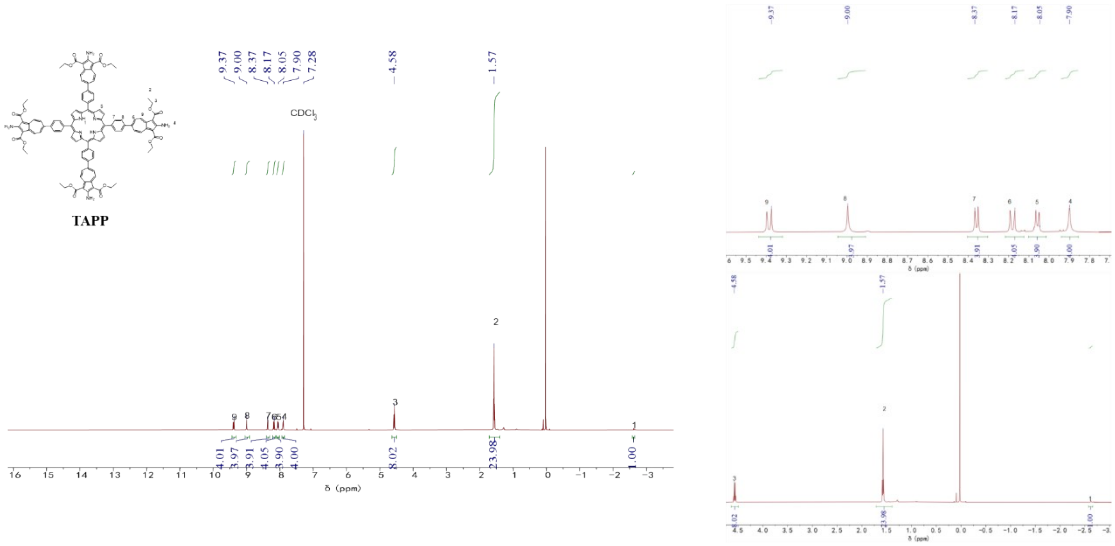

Fig. S7. ^{1}H NMR spectrum of TAPP in $CDCl_3$ at 298K.

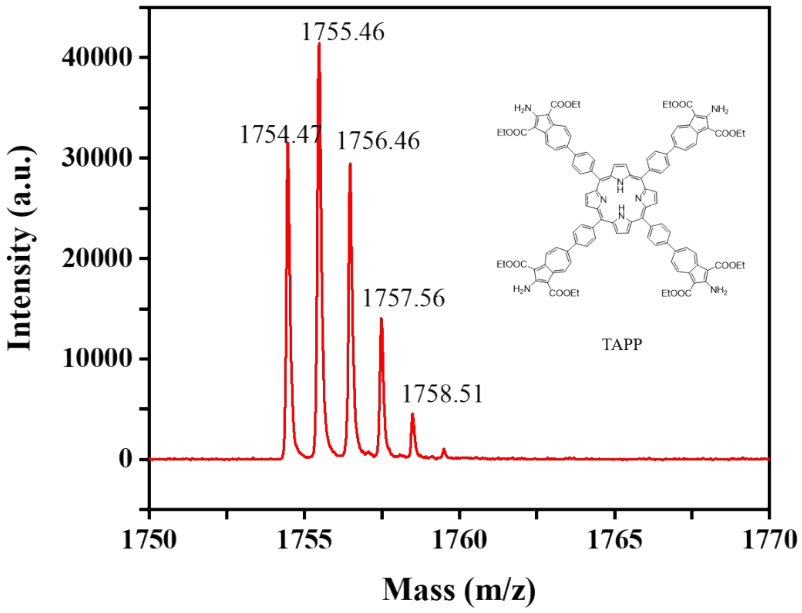

Fig. S8. Matrix–assisted laser desorption ionization time–of–flight mass spectrum of TAPP

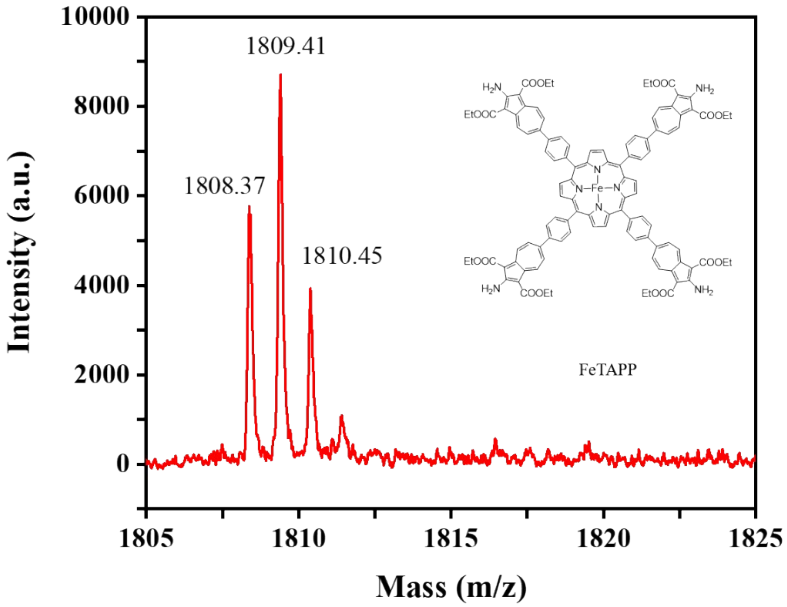

Fig. S9. Matrix–assisted laser desorption ionization time–of–flight mass spectrum of FeTAPP

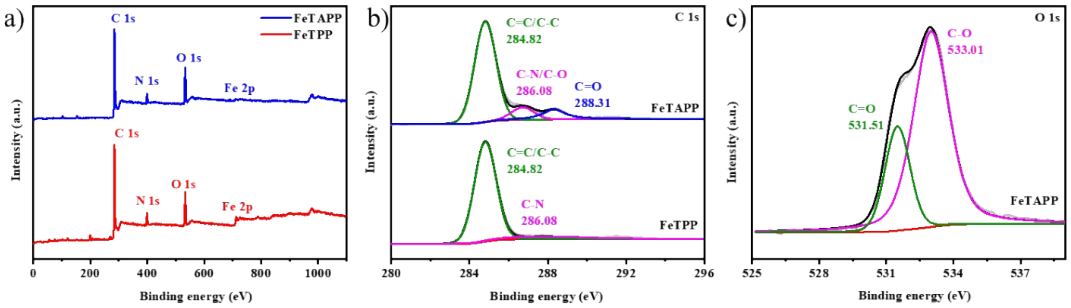

Fig. S10. a) XPS spectra of FeTAPP and FeTPP. The results reveal the existence of C, N, O and Fe elements. b) High-resolution C 1s spectra of FeTAPP and FeTPP. c) High-resolution O 1s spectra of FeTAPP and FeTPP. For C 1s spectra, the peaks at ~284.82, 286.08 and ~288.31 eV for FeTAPP, can be attributed to the C=C/C-C, C-O/C-N, and C=O, respectively. Two peaks presented at ~284.82 and 286.08 eV for FeTPP, corresponding to the C=C/C-C and C-N. For O 1s spectra, two peaks presented at ~531.51 and 533.01 eV for FeTAPP, corresponding to the C=O and C-O. The additional C–O and C=O bonds in FeTAPP come from the ester group.

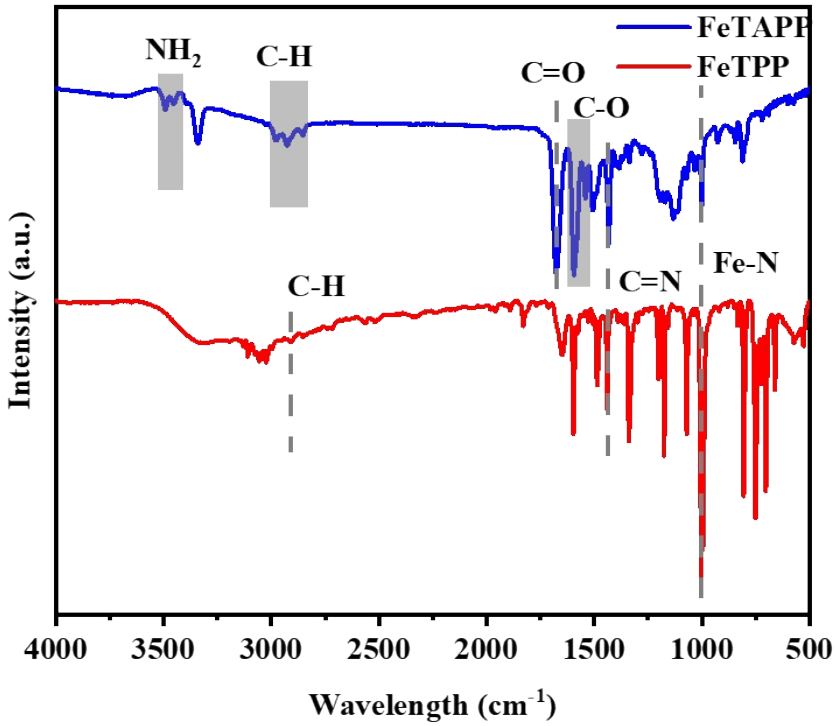

Fig. S11. FTIR spectra of FeTAPP and FeTPP. The peaks at 2841~2,982 cm^{-1} can be attributed to the C-H bond of the benzene ring, pyrrole ring and the ester group. The peaks at 1676 cm^{-1} belongs to C=O stretching vibration. The peaks at 1,504~1,586 cm^{-1} and 1,430 cm^{-1} belong to C=C stretching vibration and C=N stretching vibration, respectively. The peaks at 1,504~1,586 cm^{-1} belong to the C-O stretching vibration. The peaks 3300~3500 cm^{-1} belong to NH_2 stretching vibration.

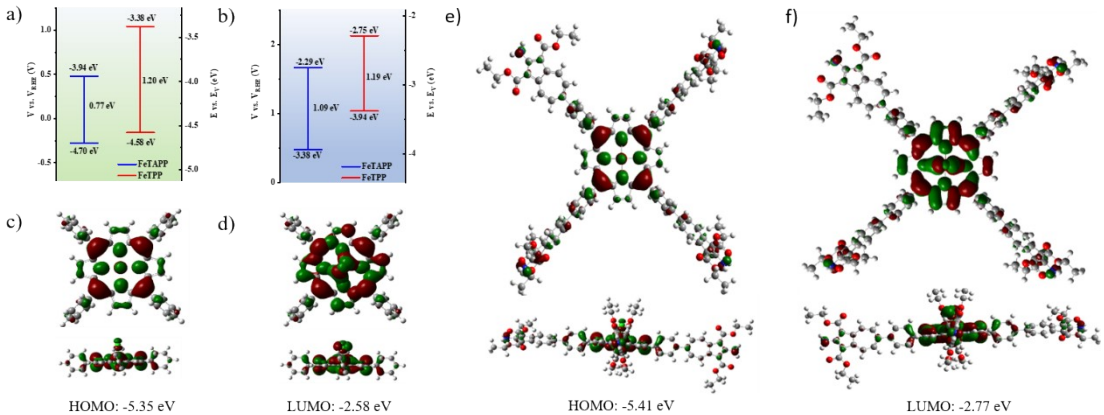

Fig. S12. a) HOMO and LUMO levels of FeTAPP and FeTPP based on CV curves. b) Optical gap of FeTAPP and FeTPP. c and d) Calculated HOMO and LUMO levels of FeTPP. e) and f) Calculated HOMO and LUMO levels of FeTAPP.

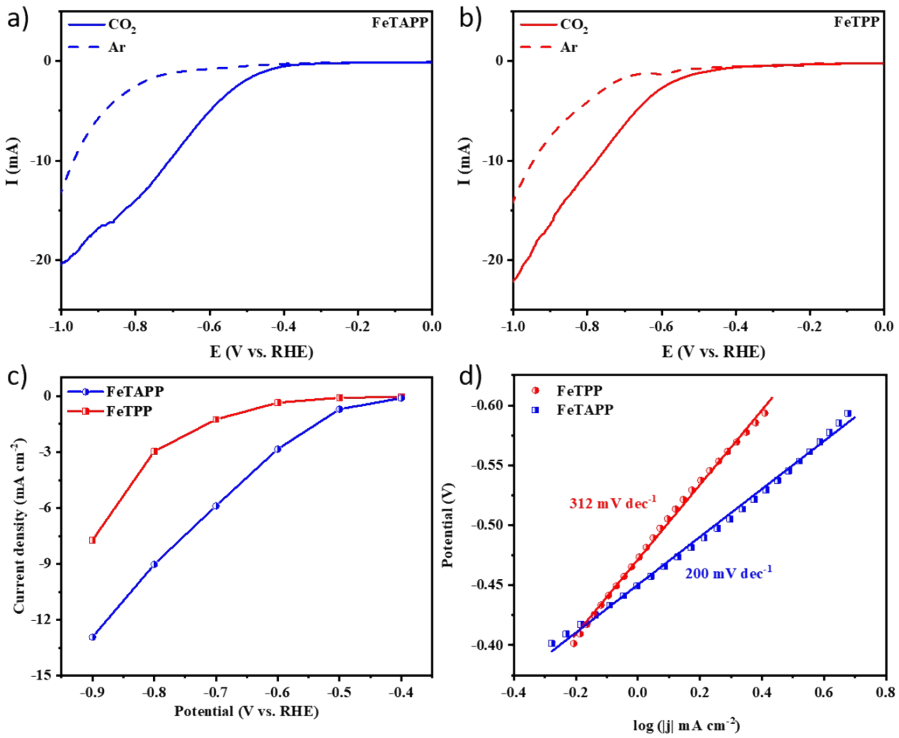

Fig. S13. The liner sweep voltammetry (LSV) curves obtained in Ar and CO_2-saturated solution (a) FeTAPP; (b) FeTPP. The current density obtained in CO_2-saturated electrolyte is larger than that in Ar-saturated electrolyte, suggesting the promising catalytic activity. c) partial current density values. d) Tafel slopes for FeTAPP and FeTPP.

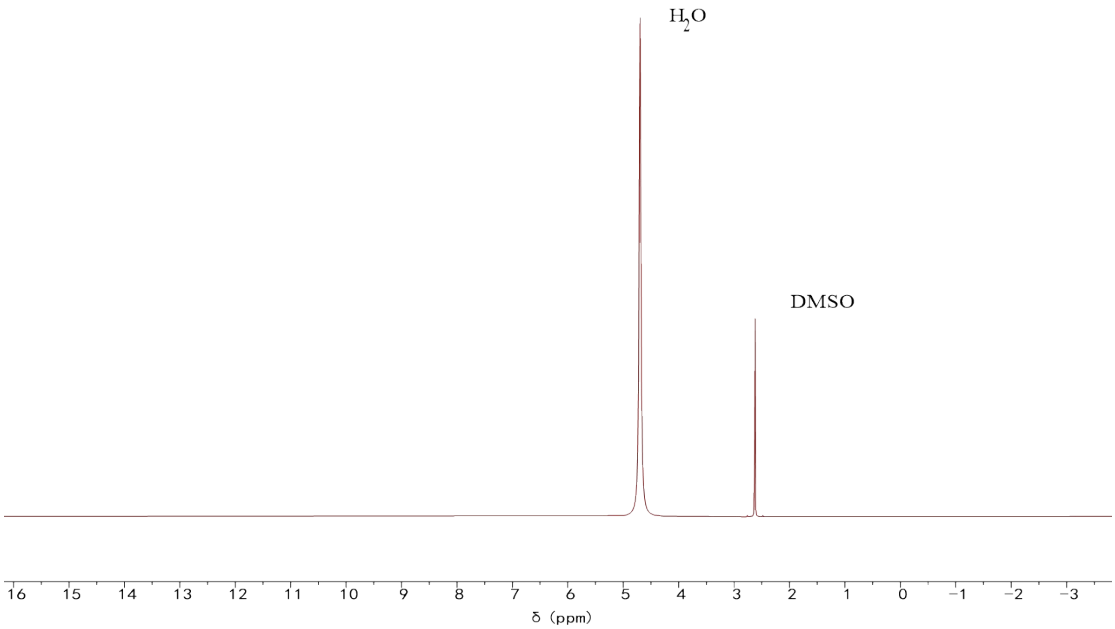

Fig. S14. ^{1}H nuclear magnetic resonance (NMR) spectroscopy for products after reaction. In addition to the water and solvent signal no additional was detected, indicating that no liquid products formation during CO_2RR.

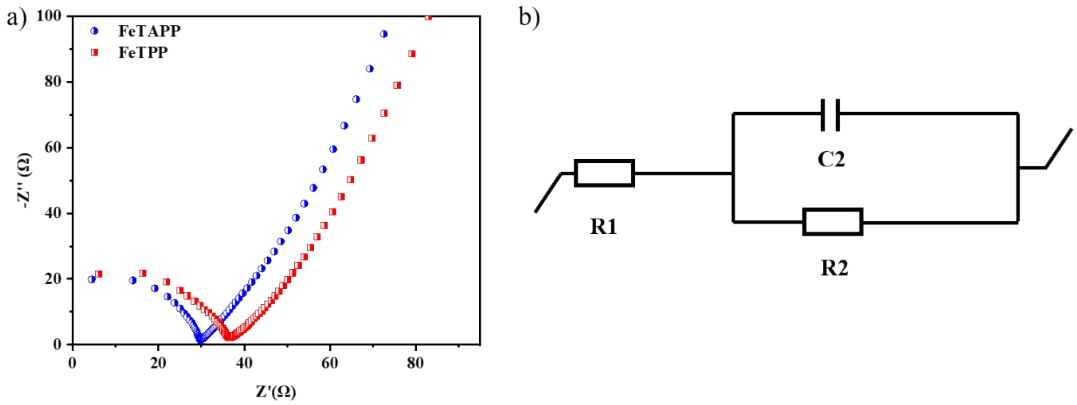

Fig. S15. a) Nyquist plots for FeTPP and FeTAPP. b) Equivalent circuit used for fitting of EIS data.

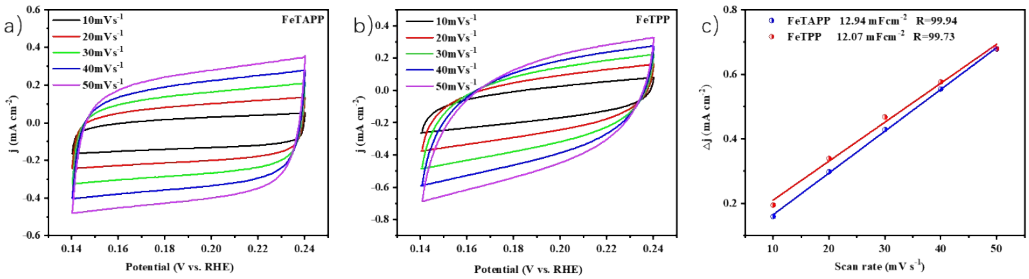

Fig. S16. a) CV curves of FeTAPP, b) CV curves of FeTPP at different scan rates (10-50 mV s^{-1}). c) Capacitive current at 0.19 V as a function of scan rate for FeTPP and FeTAPP. The double–layer capacitance of FeTAPP and FeTPP are 12.94 and 12.07 mF cm^{-2}, respectively.

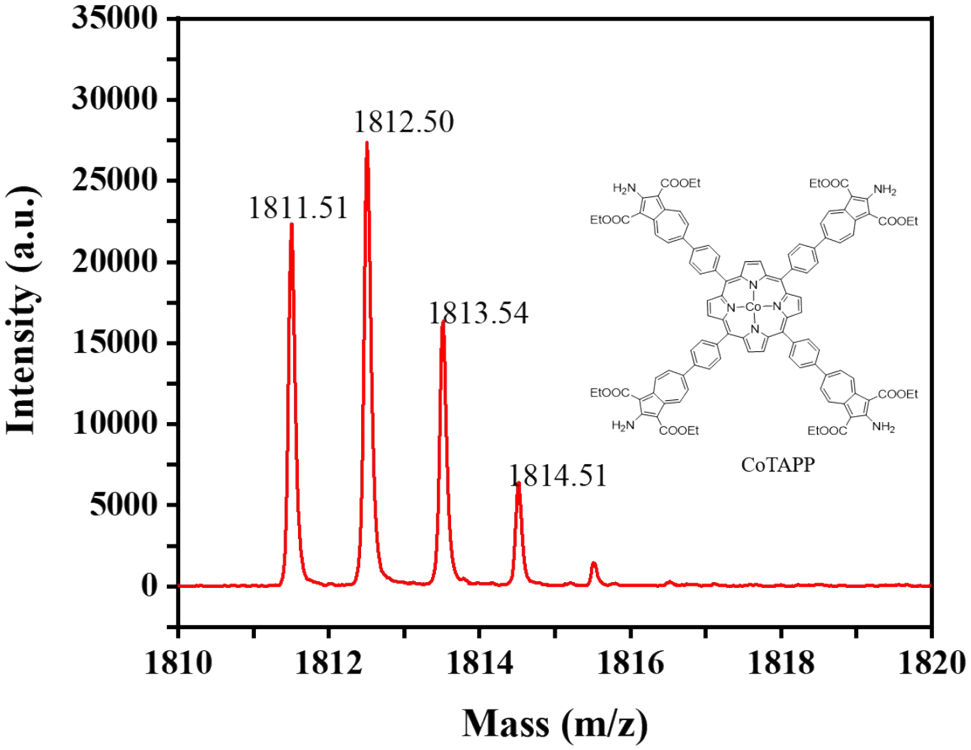

Fig. S17. MALDI-MS spectrum of CoTAPP.

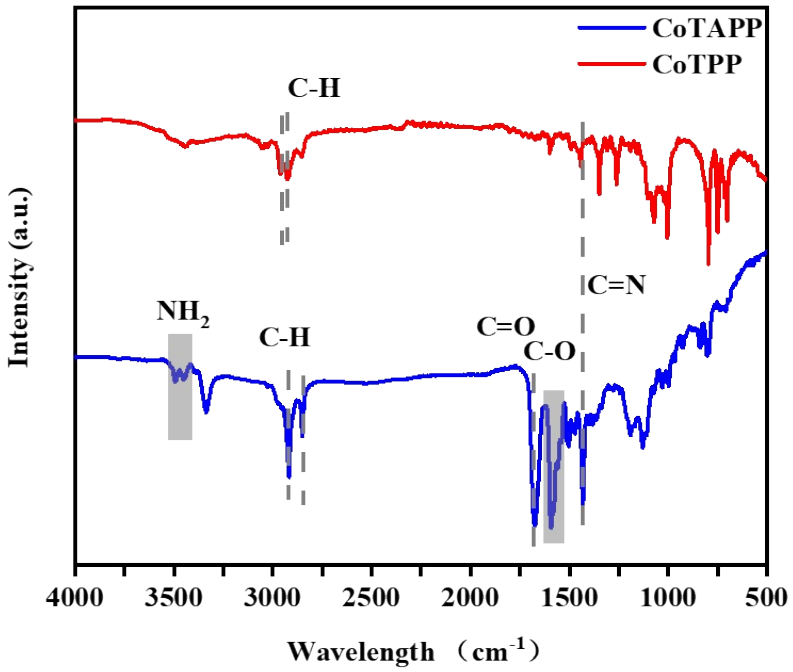

Fig. S18. FTIR spectra of CoTAPP and CoTPP. Comparing to the CoTPP result, additional -NH_2 and C=O stretching come from the side azulene group.

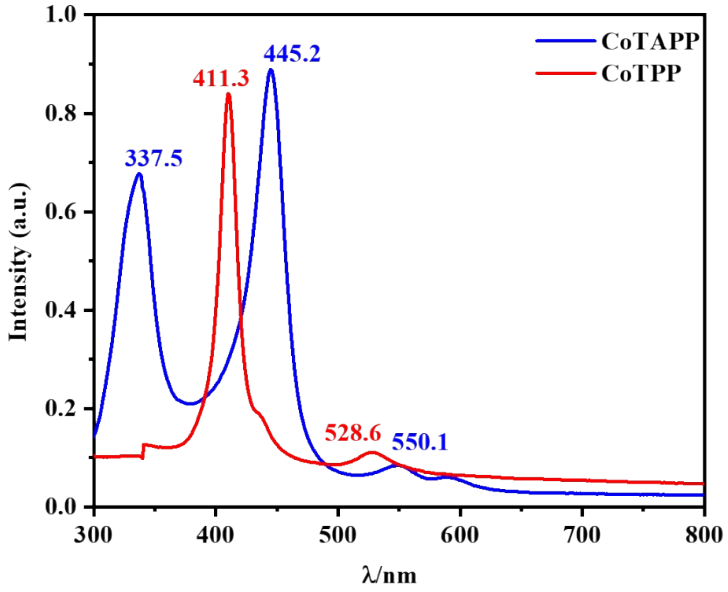

Fig. S19. UV-Vis absorption of CoTAPP and CoTPP. The spectrum of CoTPP shows two absorption peaks at approximately 416 nm and 332 nm, which can be attributed to the Soret band. In the absorption spectrum of CoTAPP, two Soret bands are observed at 337 nm and 437 nm. The band display at 337nm can be attributed to the porphyrin part, the band display at 437nm can be attributed to the azulene part. In addition, the Q band red–shift to 521 nm, suggesting a narrower HOMO/LUMO gap.

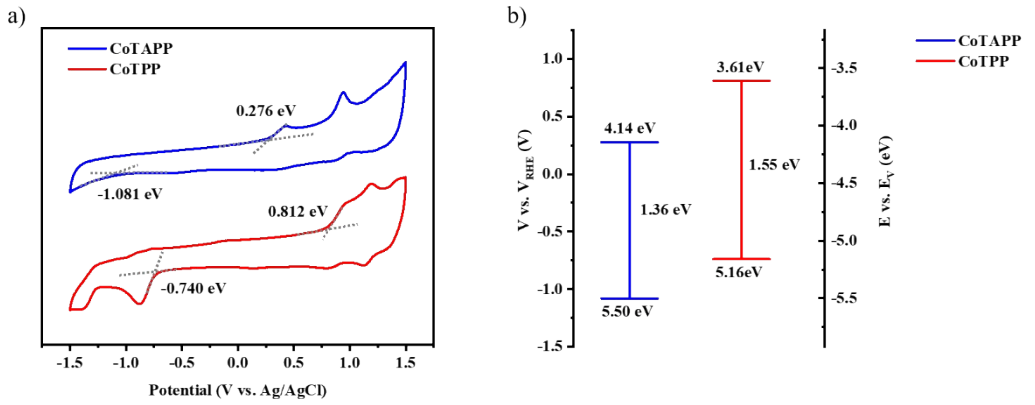

Fig. S20. Cyclic voltammetry curves of CoTAPP and CoTPP. The LUMO energy levels of CoTAPP and CoTPP are calculated to be -4.14 and -3.61 eV, respectively, and the HOMO energy levels of CoTAPP and CoTPP are calculated to be -5.50 and -5.16 eV, respectively. The HOMO/LUMO gap of CoTAPP and CoTPP are 1.36 and 1.55 eV, respectively, CoTAPP exhibits the narrower HOMO/LUMO gap than CoTPP.

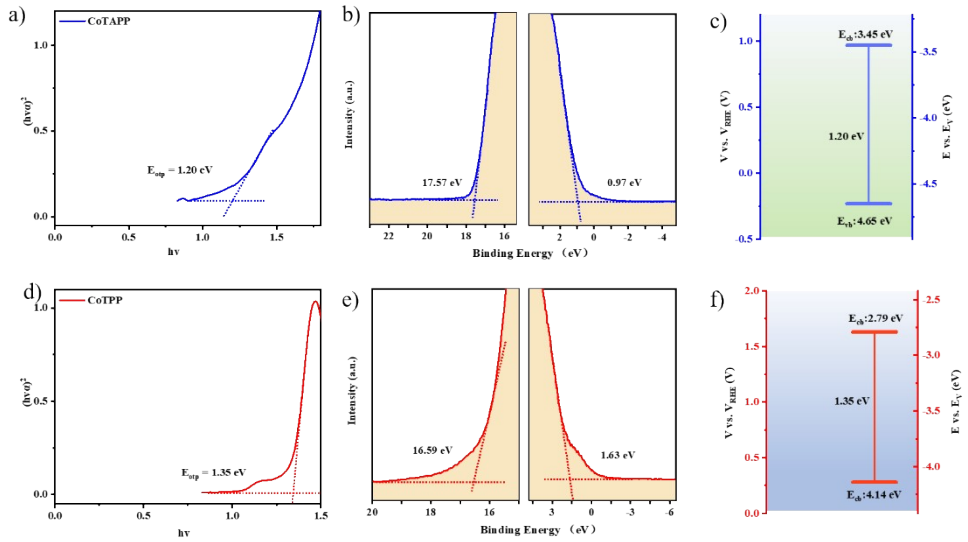

Fig. S21. a, d) *(hvα)*^{2} versus *hv* curves. The value at the intersection baseline and the tangent of the curve is the optical gap. b, e) UPS spectra of CoTAPP and CoTPP. c, f) HOMO and LUMO levels of CoTAPP and CoTPP. The optical gaps of CoTAPP and CoTPP are 1.20 and 1.35 eV, respectively. The HOMO of CoTAPP and CoTPP are -3.45 and -2.79 eV, respectively. The LUMO of CoTAPP and CoTPP are-4.05 and -4.14 eV, respectively.

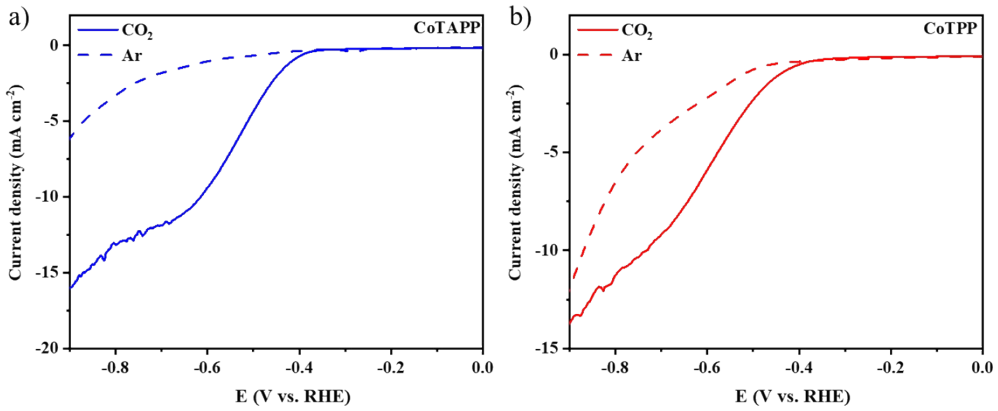

Fig. S22. The liner sweep voltammetry (LSV) curves obtained in Ar and CO_2-saturated solution (a) CoTAPP; (b) CoTPP. The current density obtained in CO_2-saturated electrolyte is larger than that in Ar-saturated electrolyte, suggesting the promising catalytic activity

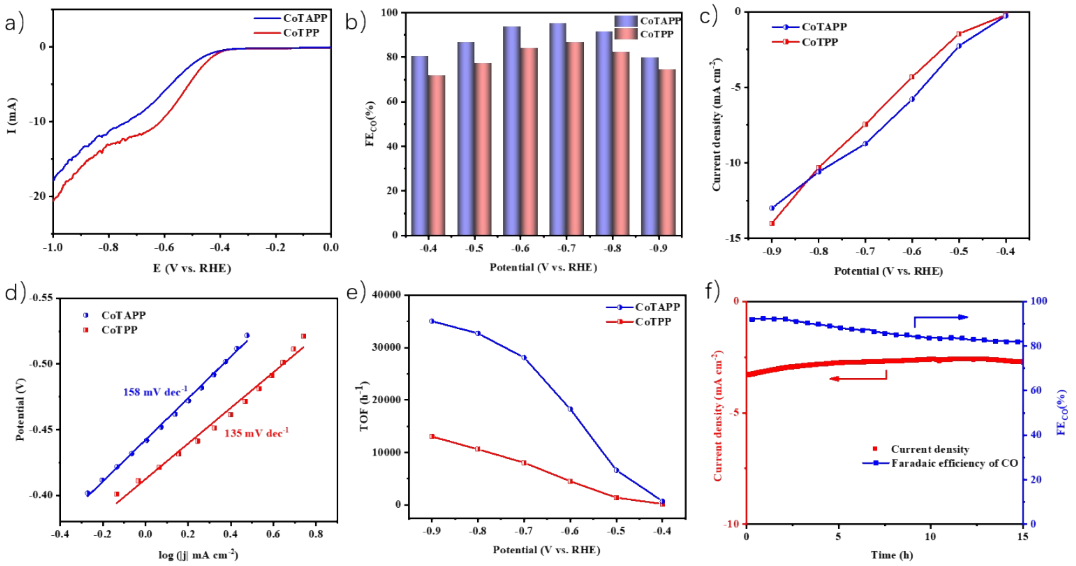

Fig. S23. CO_2RR performance of CoTAPP and CoTPP in 0.5 M $KHCO_3$. a) LSV curves for CoTAPP and CoTPP. b) CO Faradaic efficiency at various specific potentials, c) partial current density values. CoTAPP exhibits higher catalytic activity than CoTPP. d) Tafel slopes for CoTAPP and CoTPP. e) Turnover frequencies (TOF) of CoTAPP and CoTPP. The maxmum TOF of CoTAPP reaches to 35047.36 h^{-1} at -0.9V, and the TOF of CoTPP at -0.9V is 13049.07 h^{-1}. f) Long-term stability CoTAPP. CoTAPP exhibits good stability with a slight decrease in current, and the FE of CO remained about 80% after 15 hours continuous reaction.

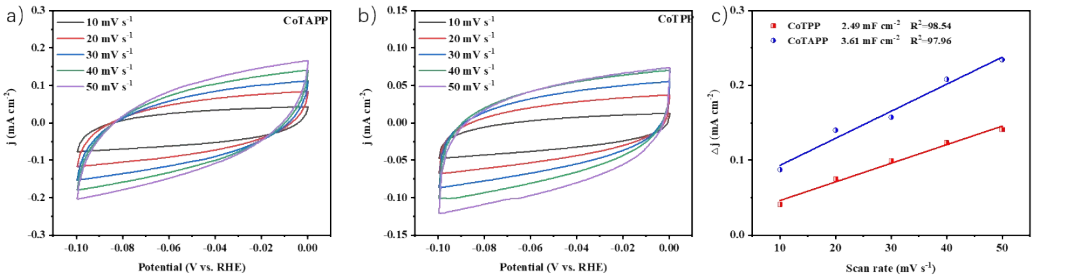

Fig. S24. a) CV curves of CoTAPP, b) CV curves of CoTPP at different scan rates (10-50 mV s^{-1}). c) Capacitive current at 0.19 V as a function of scan rate for CoTPP and CoTAPP. The double–layer capacitance of CoTAPP and CoTPP are 3.61 and 2.49 mF cm^{-2}, respectively.

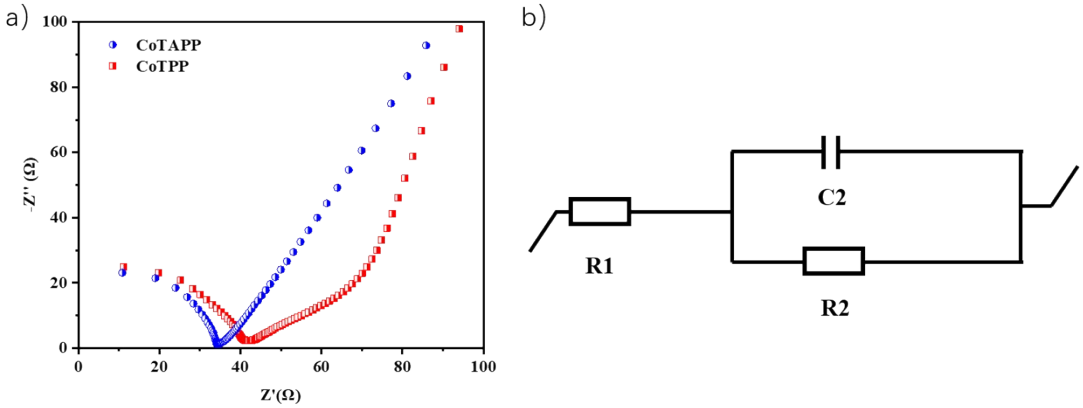

Fig. S25. a) Nyquist plots for CoTPP and CoTAPP. CoTAPP exhibits the better conductivity than CoTPP. b) Equivalent circuit used for fitting of EIS data.

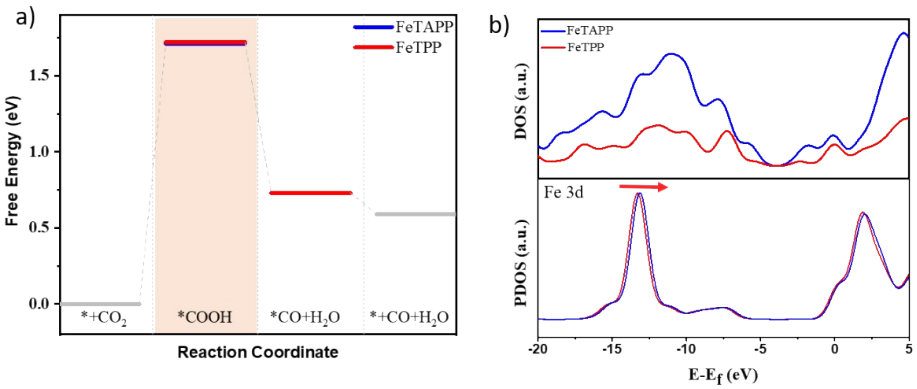

Fig. S26. a) Gibbs free energy for CO_2RR on FeTAPP and FeTPP. b) DOS and PDOS of FeTAPP and FeTPP.

Table S1. Element contents of C, O, N, and Fe for FeTAPP and FeTPP based on the XPS analysis.

	C	N	Fe	O
FeTAPP	79.59	5.36	0.53	14.52
FeTPP	79.48	6.43	1.75	12.34

Table S2. The HOMO/LUMO gap of FeTAPP and FeTPP.

		HOMO (eV)	LUMO (eV)	Eg (eV)
CV	FeTAPP	-4.70	-3.94	0.77
	FeTPP	-4.58	-3.38	1.20
UPS, UV	FeTAPP	-3.38	-2.29	1.09
	FeTPP	-3.94	-2.75	1.19
Calculated	FeTAPP	-5.41	-2.77	2.64
	FeTPP	-5.35	-2.58	2.77

Table S3. Comparison CO_2 reduction activity with reported molecular catalysts.

Catalysts	Electrolyte	j/mA cm^{-2}	V vs RHE	Main products (FE)	Ref.
FeTAPP	0.5 M $KHCO_3$	-12.9	-0.6 V	CO 99.9%	This work
FeTPP	0.5 M $KHCO_3$	-7.7	-0.6 V	CO 59.4%	This work
FePGH	0.1 M $KHCO_3$	2.3	-0.39 V	CO 96.2%	[1]
FePGF	0.1 M KCl	1.68	−0.59 V	CO 98.7%	[2]
FeTEsP	1 M H_2O in DMF		−1.55 V vs Fc+/0	HCOOH 97%	[3]
Fe-p-TMA	0.2M $NEt_4CH_3CO_2$ + 0.1 M NBu4PF6 in DMF		−0.944 V vs SHE	CO 100%	[4]
FeTPP-Cl	0.1 MTBAP/DMF,1.0 MTFE	□	2.35 Vvs. Fc/Fc+	CO 23%	[5]
FeTPP-Ur	5.5 M H_2O in DMF	0.70	-1.076 V	CO 91%	[6]
FeF20TPP	0.5 M $NaHCO_3$	~9.6	−0.5 V	CO 95%	[7]
Fe-BPPy	0.5 M $NaHCO_3$		−1.2V (vsAg/ AgCl)	CO 67.5%	[8]

Catalysts	Electrolyte	j/mA cm^{-2}	V vs RHE	Main products (FE)	Ref.
$FeFc_4$			−0.80 V vs Fc/ Fc+	CO 92%	[9]
P1-AuNP	0.5 M $KHCO_3$	2	-0.45 V	CO 93%	[10]
Fe (0)TPP	0.1 M PhOH in DMF		-1.46 V	CO 100%	[11]
FeTDHPP	2 M PhOH in DMF		-0.69 V	CO 95%	[12]
WSCAT	DMF, 0.1 M H_2O, 3 M PhOH		-1.2 vs. SCE	CO 100%	[13]
FCAT	DMF, 3 M PhOH		-1.28 V	CO 95%	[14]
Fe(0)TPP	DMF,40mM PrOH, 40mM NEt_3		- 2.4 V vs. Fc+/Fc	Formate 72%	[15]
Fe-PB	0.5 M $KHCO_3$	~1.6	-0.63 V	CO 98%-100%	[16]
CoPc-CN/CNT	0.5 M $KHCO_3$	5.6	-0.46 V	CO 88%	[17]
CoFPc	0.5 M $KHCO_3$	4.4	−0.8 V	CO 93%	[18]
CoPc-P4VP	0.1M NaH_2PO_4	2.0	-0.73 V	CO 89%	[19]
CoPc-P4VP	0.5 M $NaHCO_3$	50	-0.6 V	CO 90%	[20]
NiPcP	1 M KOH	236	-0.6 V	CO 98%	[21]
CoPc/GDY/G	0. 1 M $KHCO_3$	12	-0.9 V	CO 96%	[22]

Reference:

1. J. Choi, J. Kim, P. Wagner, S. Gambhir, R. Jalili, S. Byun, S. Sayyar, Y. M. Lee, D. R. MacFarlane, G. G. Wallace and D. L. Officer, *Energy Environ. Sci.*, 2019, **12**, 747-755.

2. J. Choi, P. Wagner, R. Jalili, J. Kim, D. R. MacFarlane, G. G. Wallace and D. L. Officer, *Adv. Energy Mater.*, 2018, **8**, 1801280.

3. S. Amanullah, P. Saha and A. Dey, *J. Am. Chem. Soc*., 2021, **143**, 13579–13592.

4. I. Azcarate, C. Costentin, M. Robert and J.-M. Savéant, *J. Am. Chem. Soc.*, 2016, **138**, 16639-16644.

5. S. Masaoka, K. Kosugi and M. Kondo, *Angew. Chem. Int. Ed.*, 2021, **60 (40)**, 22070-22074.

6. P. Gotico, B. Boitrel, R. Guillot, M. Sircoglou, A. Quaranta, Z. Halime, W. Leibl and A. Aukauloo, *Angew. Chem., Int. Ed.*, 2019, **58**, 4504-4509.

7. X. Lu, H. A. Ahsaine, B. Dereli, A. T. Garcia-Esparza, M. Reinhard, T. Shinagawa, D. Li, K. Adil, M. R. Tchalala, T. Kroll, M. Eddaoudi, D. Sokaras, L. Cavallo and K. Takanabe, *ACS Catal.*, 2021, **11**, 6499-6509.

8. M. Tasaki, Y. Okabe, H. Iwami, C. Akatsuka, K. Kosugi, K. Negita, S. Kusaka, R. Matsuda, M. Kondo and S. Masaoka, *small.*, 2021, **17**, 2006150.

9. B. Mondal, P. Sen, A. Rana, D. Saha, P. Das and A. Dey, *ACS Catal.*,2019, **9**, 3895-3899.

10. Z. Cao, S. B. Zacate, X. Sun, J. Liu, E. M. Hale, W. P. Carson, S. B. Tyndall, J. Xu, X. Liu, X. Liu, C. Song, J.-h. Luo, M.-J. Cheng, X. Wen and W. Liu, Angew. *Chem., Int. Ed*., 2018, **57**, 12675-12679.

11. C. Costentin, S. Drouet, G. Passard, M. Robert and J.-M. Savéant, J. Am. Chem. Soc., 2013, 135, 9023-9031.

12. C. Costentin, S. Drouet, M. Robert and J.-M. Savéant, *Science*, 2012, **338**, 90-94.

13. C. Costentin, M. Robert, J.-M. Savéant and A. Tatin, *J. Am. Chem. Soc.*, 2015, **112**, 6882-6886.

14. C. Costentin, G. Passard, M. Robert and J.-M. Savéant, *J. Am. Chem. Soc.*, 2014, **136**, 11821-11829.

15. C. G. Margarit, N. G. Asimow, C. Costentin and D. G. Nocera, *ACS Energy Lett.*, 2020, **5**, 72-78.

16. P. T. Smith, B. P. Benke, Z. Cao, Y. Kim, E. M. Nichols, K. Kim and C. J. Chang, *Angew. Chem., Int. Ed.*, 2018, **57**, 9684-9688.

17. X. Zhang, Z. Wu, X. Zhang, L. Li, Y. Li, H. Xu, X. Li, X. Yu, Z. Zhang, Y. Liang and H. Wang, *Nat. Commun.*, 2017, **8**, 14675.

18. N. Morlanés, K. Takanabe and V. Rodionov, *ACS Catal.*, 2016, **6**, 3092-3095.

19. W. W. Kramer and C. C. L. McCrory, *Chem. Sci.*, 2016, **7**, 2506-2515.

20. N. Han, Y. Wang, L. Ma, J. Wen, J. Li, H. Zheng, K. Nie, X. Wang, F. Zhao, Y. Li, J. Fan, J. Zhong, T. Wu, D. J. Miller, J. Lu, S.-T. Lee and Y. Li, *Chem*, 2017, **3**, 652-664.

21. S. Wei, H. Zou, W. Rong, F. Zhang, Y. Ji and L. Duan, *Appl. Catal.*, B, 2021, **284**, 119739.

22. H. Gu, L. Zhong, G. Shi, J. Li, K. Yu, J. Li, S. Zhang, C. Zhu, S. Chen, C. Yang, Y. Kong, C. Chen, S. Li, J. Zhang and L. Zhang, *J. Am. Chem. Soc.*, 2021, **143**, 8679-8688.